ADVANCES IN ATMOSPHERIC SCIENCES, VOL. 28, NO. 6, 2011, 1336–1344

Radiative Forcing and Climate Response Due to Black Carbon in Snow and Ice

WANG Zhili[1,2,3] (王志立), ZHANG Hua*[3] (张 华), and SHEN Xueshun[4] (沈学顺)

[1] *Center for Atmosphere Watch and Services, Chinese Academy of Meteorological Sciences, China Meteorological Administration, Beijing* 100081

[2] *Graduate University of Chinese Academy of Sciences, Beijing* 100049

[3] *National Climate Center, China Meteorological Administration, Beijing* 100081

[4] *State Key Laboratory of Severe Weather, Chinese Academy of Meteorological Sciences, Beijing* 100081

(Received 9 December 2010; revised 14 April 2011)

ABSTRACT

The radiative forcing and climate response due to black carbon (BC) in snow and/or ice were investigated by integrating observed effects of BC on snow/ice albedo into an atmospheric general circulation model (BCC_AGCM2.0.1) developed by the National Climate Center (NCC) of the China Meteorological Administration (CMA). The results show that the global annual mean surface radiative forcing due to BC in snow/ice is +0.042 W m^{-2}, with maximum forcing found over the Tibetan Plateau and regional mean forcing exceeding +2.8 W m^{-2}. The global annual mean surface temperature increased 0.071°C due to BC in snow/ice. Positive surface radiative forcing was clearly shown in winter and spring and increased the surface temperature of snow/ice in the Northern Hemisphere. The surface temperatures of snow-covered areas of Eurasia and North America in winter (spring) increased by 0.83°C (0.6°C) and 0.83°C (0.46°C), respectively. Snowmelt rates also increased greatly, leading to earlier snowmelt and peak runoff times. With the rise of surface temperatures in the Arctic, more water vapor could be released into the atmosphere, allowing easier cloud formation, which could lead to higher thermal emittance in the Arctic. However, the total cloud forcing could decrease due to increasing cloud cover, which will offset some of the positive feedback mechanism of the clouds.

Key words: black carbon, snow/ice, radiative forcing, climate effects

Citation: Wang, Z. L., H. Zhang, and X. S. Shen, 2011: Radiative forcing and climate response due to black carbon in snow and ice. *Adv. Atmos. Sci.*, **28**(6), 1336–1344, doi: 10.1007/s00376-011-0117-5.

1. Introduction

Black carbon (BC), an important component of atmospheric aerosols, is produced by the incomplete combustion of hydrocarbon-containing materials including fossil fuels, biofuels, and biomass (IPCC, 2001; 2007). Bond et al. (2004) estimated the total global emission of BC to be ∼8 Tg C yr^{-1}, with contributions of 4.6 Tg C yr^{-1} from fossil fuel and biofuel combustion and 3.3 Tg C yr^{-1} from open biomass burning. Four main areas are large sources of BC: Eastern China, Western Europe, South America, and central Africa. Other important sources are southern North America and Australia (Streets et al., 2003; IPCC, 2007). Not only can BC directly alter the radiation balance of Earth's atmospheric system, it may also indirectly affect regional or global climate by changing the microphysical properties of clouds in terms of cloud condensation nuclei (CCN) or ice nuclei (IPCC, 2007; Wang et al., 2009; Zhang et al., 2009). BC in air can be transported long distances by atmospheric circulation and deposited onto snow and/or ice surfaces by rainout, washout, and dry deposition. Even very small quantities of BC can reduce the albedo of

*Corresponding author: ZHANG Hua, huazhang@cma.gov.cn

snow/ice because of the high albedo of pristine snow at visible wavelengths, the multiple scattering properties of snowpack, and the large difference of mass absorption coefficients between BC and snow/ice (Warren and Wiscombe, 1980; Flanner et al., 2007). Reduced albedo means increased absorption of solar radiation by the snow/ice and thus accelerated melting (referred to as the "snow/ice albedo mechanism") (Hansen and Nazarenko, 2004; Jacobson, 2004; Flanner et al., 2007).

A number of studies have measured BC concentrations in snow/ice and have analyzed the effects of BC on surface albedo (e.g., Warren, 1982; Noone and Clarke, 1988; Grenfell et al., 2002). Warren and Wiscombe (1980) found that snow albedo may be reduced by 1% if the BC concentration reaches 15 ng g^{-1}. Light et al. (1998) calculated that sea-ice albedo could be reduced by up to 30% with a BC concentration of 150 ng g^{-1}. In the Tibetan Plateau region, large amounts of BC attach to the snow and/or ice, increasing the absorption of solar radiation and the thermal radiation emission from the Earth. The results measured by Xu et al. (2006) showed that the highest mean BC content in snow/ice was 79.2 ng g^{-1} in the northeast Himalaya, and the lowest content was 4.3 ng g^{-1} in the western Himalaya. Ming et al. (2008) reported that the average BC concentration in snow/ice of the Everest region from 1951 to 2001 was ∼16 ng g^{-1} and the largest radiative forcing by BC in snow/ice in the summer of 2001 exceeded +4.5 W m^{-2}. In many snow-covered regions in the Northern Hemisphere, snow and ice begin to melt heavily in March and April, but because these months precede the agricultural season, tremendous amounts of snow/ice water resources are lost before they can be used (Thompson et al., 2003; Barnett et al., 2005). Snow is an important source of surface runoff and soil moisture. Changes in the radiative properties of snow can thus have important impacts on the radiation balance and the water balance of the Earth's surface and the hydrological cycle. From a global perspective, the decrease of snow/ice albedo due to BC and the resultant rise in surface temperature can accelerate the global melting of glaciers and can contribute greatly to global warming. The effects of BC in snow/ice on radiative flux have also been simulated using climate models (Hansen and Nazarenko, 2004; Hansen et al., 2007; Flanner et al., 2007; Koch et al., 2009; Rypdal et al., 2009). Those studies estimated that global annual mean radiative forcing due to BC in snow/ice ranges between +0.007 and +0.16 W m^{-2}, and they showed that the efficacy of climate forcing to change global surface temperature by the snow/ice albedo mechanism is higher than that of CO_2. Some uncertainties about this research remain, such as limited observational data, mixed states of BC and snow/ice particles, different parameterizations of models, and so on. The IPCC (2007) also indicated that the level of scientific understanding of the forcing by BC in snow/ice is still low, and that further studies are therefore needed.

In the present study, radiative forcing by BC in snow/ice and the climate response to this forcing were studied using the second-generation AGCM developed by the National Climate Center (NCC) of the China Meteorological Administration (CMA), called the BCC_AGCM2.0.1. Section 2 describes the model and experimental design. Section 3 contains the calculation methods of the radiative forcing of BC in snow/ice and analyzes its effect on global climate. Finally, conclusions and discussion are presented in section 4.

2. Model Description and Experimental Design

2.1 *Basic model description*

The BCC_AGCM2.0.1 was developed by the National Climate Center of the China Meteorological Administration (NCC/CMA) based on the Community Atmosphere Model Version 3 (CAM3) of the U.S. National Center for Atmospheric Research (NCAR). The model uses horizontal triangular truncation at wavenumber 42 (T42, ∼2.8°×2.8°) and a vertical hybrid σ-pressure coordinate, which includes 26 vertical layers with the top layer at a pressure of 2.9 hPa. The model uses the same radiation scheme as that used in CAM3; both models divide the whole shortwave region into 19 spectral bands and use a two-stream δ-Eddington approximation (Briegleb, 1992). This scheme takes atmospheric absorption due to gases such as H_2O, CO_2, O_3, and O_2 into account and also considers multiple-scattering and absorption processes due to aerosols such as sulfate, BC, organic carbon, dust, and sea salt. The model was coupled with the Community Land Model (CLM3), in which snow is a forecast variable. The simulation of snow takes into account the interactions between snowfall and melting and between new snow and old snow, as well as the integration, compression, and deformation processes among snow layers (Oleson et al., 2004). The sea-ice concentration and thickness are prescribed in the model. The shortwave region is divided into two spectral bands in the CLM3 and the sea-ice model including visible $\lambda<0.7$ μm and near-infrared $\lambda\geqslant 0.7$ μm. Monthly mean climatological data from 1971 to 2000 on a Gaussian grid, obtained from National Centers for Environmental Prediction (NCEP) reanalysis products, were used as the initial

model field, and the geographical distribution of sea surface temperature was prescribed based on the 21-year climatology for 1981–2001 (available online from http://www/ccsm.ucar.edu/models/atmcam/docs/description). The climatologic field of the aerosol species considered in this study used monthly mean aerosol mass concentrations from the Model for Atmospheric Chemistry to Transport (MATCH) (Rasch et al., 1997), and their optical properties were described by Zhang et al. (2009). The aerosol distribution reasonably agreed with observations (Collins et al., 2001, 2002).

Compared with CAM3, many parameterizations were changed in BCC_AGCM2.0.1. The dynamics in the model differ significantly from the Eulerian spectral formulation of the dynamical equations in CAM3, and a reference stratified atmospheric temperature and a reference surface pressure were introduced into the model governing equations to improve calculation of the pressure gradient force and the gradients of surface pressure and temperature (Wu et al., 2010). The major modifications to the model physics include a new convection scheme (Zhang and Mu, 2005), a dry adiabatic adjustment scheme in which potential temperature is conserved (Yan, 1987), a modified scheme to calculate sensible heat and moisture fluxes over open

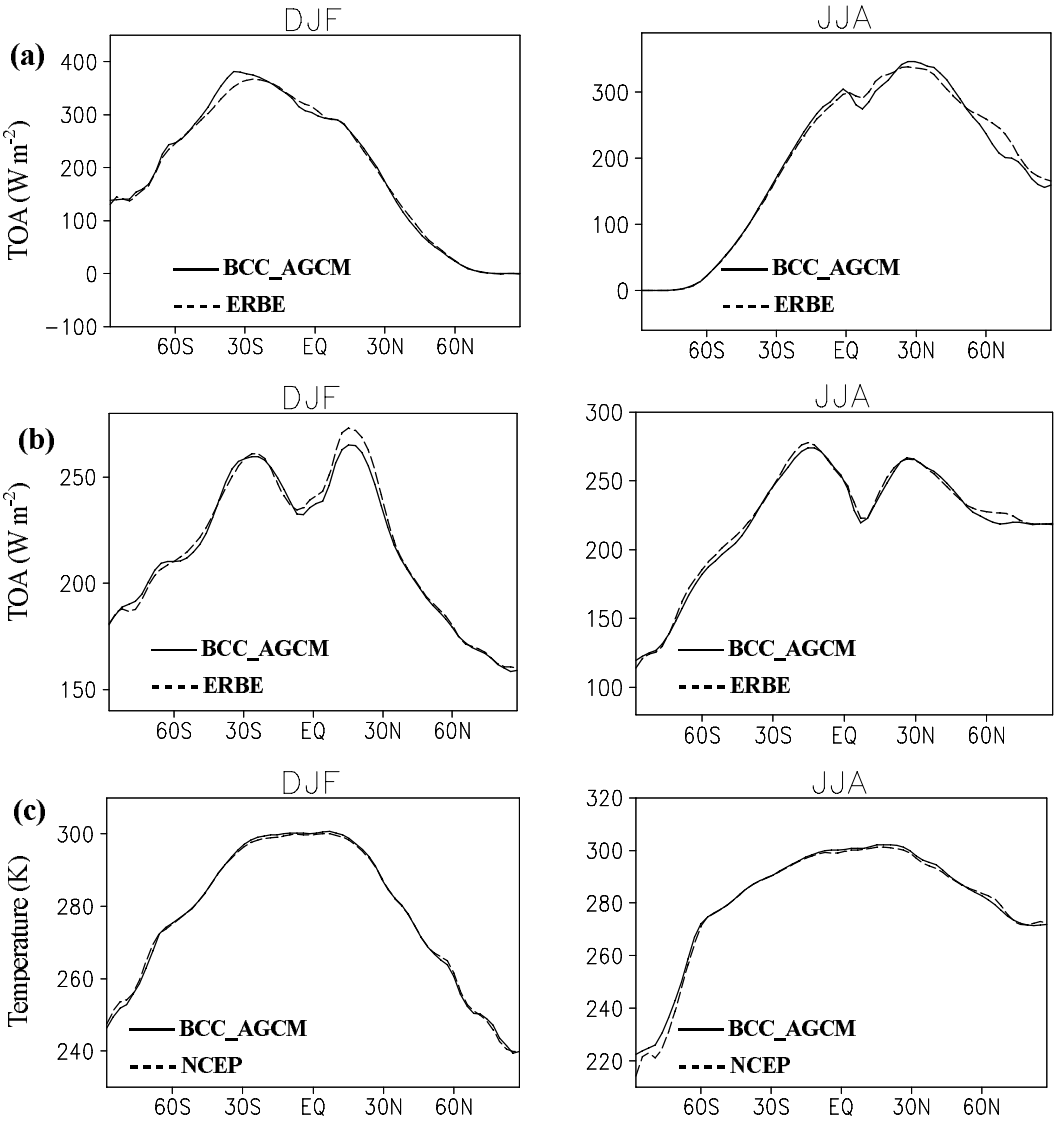

Fig. 1. The comparison of zonal mean of (a) net shortwave flux at the TOA (units: W m^{-2}), (b) upward longwave flux at the TOA (units: W m^{-2}), and (c) surface temperature (units: K) between the simulation and observations/reanalysis data. DJF and JJA represent winter and summer, respectively.

ocean that considers the effect of ocean waves on latent and sensible heat fluxes (Wu et al., 2010), and an empirical equation to compute the snow cover fraction (Wu and Wu, 2004). The model provides overall improvements to climate simulation in comparison with CAM3, especially for simulating the tropical maximum and the subtropical minimum of precipitation, wind stress, and sensible and latent heat fluxes at the ocean surface (Wu et al., 2010; Wang et al., 2010). Figure 1 gives the seasonal changes of the zonal mean of net shortwave flux and upward longwave flux at the top of the atmosphere (TOA) and surface temperature simulated by BCC_AGCM2.0.1. For comparison, observations from the Earth Radiation Budget Experiment (ERBE; Harrison et al., 1990) and reanalysis data from National Center for Environmental Prediction (NCEP; Kistler et al., 2001) are also presented. As shown in Fig. 1, latitudinal and seasonal patterns of the simulation are consistent with the observations or the NCEP data, and there are no large differences between them except that the simulated net shortwave flux at the TOA in summer (June, July, August: JJA) in the high-latitude region and the simulated upward longwave flux at the TOA in winter (December, January, February: DJF) in the tropical region in the Northern Hemisphere were underestimated in comparison with ERBE data.

2.2 *Experimental design*

Observations and simulations have shown that the effects of BC on snow/ice albedo are mainly concentrated at wavelengths <0.9 μm (Warren and Wiscombe, 1980; Jacobson, 2004; Flanner et al., 2007). Hansen and Nazarenko (2004) summarized the BC amounts in snow/ice samples from various sites in Alaska, Canada, Greenland, Sweden, and Eurasia, and in the sea ice of the central Arctic. They calculated the effects of BC on snow/ice albedo in the different regions and found that, with wavelength λ<0.77 μm, snow/ice albedos were reduced by 2.5% at the Arctic, by 5% for land-surface snow in the Northern Hemisphere, and by 1% for snow/ice in the Southern Hemisphere except at the South Pole. Ming et al. (2009) also analyzed the effects of BC in snow/ice on albedo at many sites in western China and the Tibetan Plateau. Their results showed albedo reduction due to BC in snow/ice of 6% at Haxilegen (43.73°N, 84.46°E) and Miaoergou (43.06°N, 94.32°E), 5% at Lanong (30.42°N, 90.57°E), and 4% at Mushitage (38.28°N, 75.02°E). The mean reduction of albedo among these sites was close to 5% in visible, which was consistent with the results of Hansen and Nazarenko (2004).

Firstly, two simulation experiments were conducted in this study to examine the climate response due to BC in snow/ice. In the control experiment (EXP1), no effect of BC on the snow/ice albedo was included. In the second experiment (EXP2), albedo decrease in snow/ice was specified at λ<0.7 μm according to the calculated results of Hansen and Nazarenko (2004) and Ming et al. (2009) described above (i.e., the snow/ice albedo in the Arctic decreased by 2.5%; the snow albedo on land in the Northern Hemisphere decreased by 5%, and the snow/ice albedo in the Southern Hemisphere, except the South Pole, decreased by 1%). In EXP2, the instantaneously radiative forcing caused by BC in snow/ice was also calculated. In addition, we conducted another experiment (EXP3) to calculate the instantaneously radiative forcing when simultaneously considering the BC in snow/ice and in the atmosphere. The difference between the results of the EXP1 and EXP2 was regarded as the effect of BC in snow/ice on climate. In each experiment, we ran the BCC_AGCM2.0.1 for 11 years, with the first year as the spin-up time. The results for the last 10 years were averaged and analyzed for this study.

3. Results

3.1 *Surface radiative forcing (F_s) of BC in snow/ice*

Figure 2a shows the annual mean distribution of BC column burden used in this model. The largest column burden of BC occurs over East Asia with a maximum value >2.7 mg m^{-2}. This high value was most likely attributed to a rapid industrial development in southeastern China in recent years. Other regions with large column burdens include India, Western Europe, some of the west coast of Central Africa, and central South America. There was also a relatively high column burden in the southern part of North America and in Australia.

BC deposits on snow/ice surfaces reduce their albedo and increase their absorption of solar radiation, so that positive radiative forcing is produced on the Earth's surface. The annual mean distribution of surface radiative forcing shown in Fig. 2b reveals that the maximum forcing in the Northern Hemisphere occurs over the Tibetan Plateau (30°–40°N, 80°–100°E), where regional mean forcing reaches +2.8 W m^{-2}, which is similar to the result calculated by Flanner et al. (2007) using BC emission list data (Bond et al., 2004). The maximum radiative forcing on Greenland also exceeds +2.0 W m^{-2}. At the two major regions of snow cover in Eurasia and North America, the annual mean surface radiative forcing is +0.2 W m^{-2} to +2.0 W m^{-2}. The mean value for sea ice at the Arctic pole is approximately +0.8 W m^{-2}, and forcing is also distributed with a small range in the

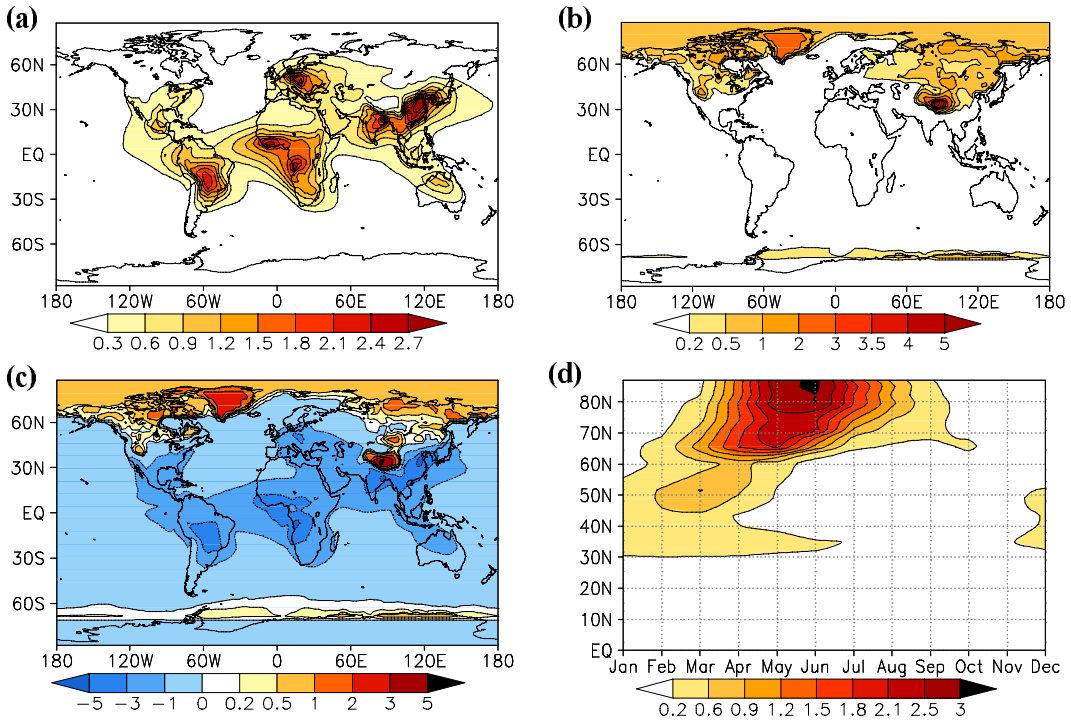

Fig. 2. Annual mean distribution of (a) BC column burden (units: mg m^{-2}), (b) surface radiative forcing due to BC in snow/ice and (c) BC in snow/ice and atmosphere, and (d) the seasonal change of zonal mean surface radiative forcing due to BC in snow/ice (units: W m^{-2}).

Southern Hemisphere. The global annual mean of surface radiative forcing calculated in this study was +0.042 W m^{-2}, which is smaller than the result of Hansen and Nazarenko (2004).

Figure 2c shows the annual mean distribution of total surface radiative forcing due to BC in snow/ice and in atmosphere. When simultaneously considering the BC in the atmosphere, the ranges of positive surface forcing greatly decrease in Eurasia and North America, but it barely affects the forcing in Tibetan Plateau and the Arctic pole, where the regional annual mean forcing rates are +2.5 W $m^{-2}$and +0.7 W m^{-2}, respectively.

The magnitude of surface radiative forcing by BC in snow/ice is determined by the concentration of BC in the snow/ice, the surface-incident solar flux, and the snow cover (Flanner et al., 2007). The seasonal change of zonal mean surface radiative forcing by BC in snow/ice is shown in Fig. 2d. Distinct forcing is shown in the region 30°–50°N in winter; over time, large values of radiative forcing gradually move northward with large amounts of solar radiation flux and snow cover. In summer, the radiative forcing at high-latitude areas of the Northern Hemisphere reach their maximum values (>+1.8 W m^{-2} in most regions) due to the large amounts of BC emissions and the accumulation of BC by melting snow. Although the BC concentration in snow/ice is low and the surface-incident solar flux drops in the Arctic, the zonal mean values and range of radiative forcing are still large due to the large extent of snow/ice cover. In autumn, although BC emission is still high, radiative forcing is very small because snow pack has not yet accumulated.

3.2 *Climate response*

The effects on annual mean surface temperature from BC in snow/ice are shown in Fig. 3. The surface

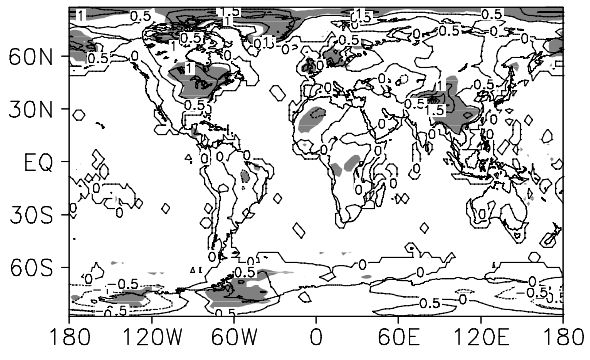

Fig. 3. The effect of BC in snow/ice on annual mean surface temperature (units: °C) (The shaded areas shows the confidence exceeds 95% using a *t*-test).

temperatures of snow-covered areas on land and of sea-ice-covered areas show an obvious increase due to the enhanced absorption of solar radiation caused by BC in snow/ice. The mean surface temperature of snow/ice on the Tibetan Plateau, the area with the largest radiative forcing, increased by 1.6°C. At the two major snow-covered regions of Eurasia and North America, temperature increases were ∼0.5°C and were >1°C in northern Canada and the eastern United States. In the area of Arctic sea-ice cover, a temperature increase of 1°C is shown. Furthermore, the results indicate that global annual mean surface temperature increased by ∼0.071°C due to BC in snow/ice. The changes of simulated surface temperature exceeded the 95% confidence level (t-test) over most areas of the Arctic sea ice, Tibetan Plateau, and North America. In China, recent observational studies have also shown that >80% of glaciers are receding (Xiao et al., 2007). Increased surface temperatures due to BC in snow/ice will further accelerate the melting of snow/ice under global warming due to CO_2.

Garrett and Zhao (2006) pointed out that anthropogenic aerosol could be transported to the Arctic through atmospheric circulation and could change the microphysical and radiative properties of clouds there, leading to an increase in surface longwave fluxes and contributing to the rise of Arctic surface temperatures. Figure 4a shows the effect of BC in snow/ice on annual zonal means of total cloud cover and net longwave flux at the surface. As shown in this figure, BC in snow/ice can also lead to an increase in surface longwave flux in the Arctic, where the maximum value exceeds +1 W m^{-2} at 85°N. This increase is due to the warmer surface temperature, which causes more water vapor to be released into the atmosphere, allowing for easier cloud formation, which could result in higher thermal emittance arriving at the surface in the Arctic. Consequently, this positive feedback mechanism will further accelerate Arctic warming. But increasing cloud cover will decrease net cloud forcing in the Arctic (Fig. 4b), and this will offset some of the positive feedback mechanism of clouds.

Figure 5 presents the seasonal changes of zonal mean differences of surface temperature and snowmelt rate caused by BC in snow/ice. The temporal and spatial distributions of the differences of surface temperature and snowmelt rate are very consistent with those of surface radiative forcing. With the emergence of surface positive radiative forcing in winter, surface temperature significantly increased on land areas with snow/ice cover in the Northern Hemisphere. The mean increase in the surface temperature of snow in winter

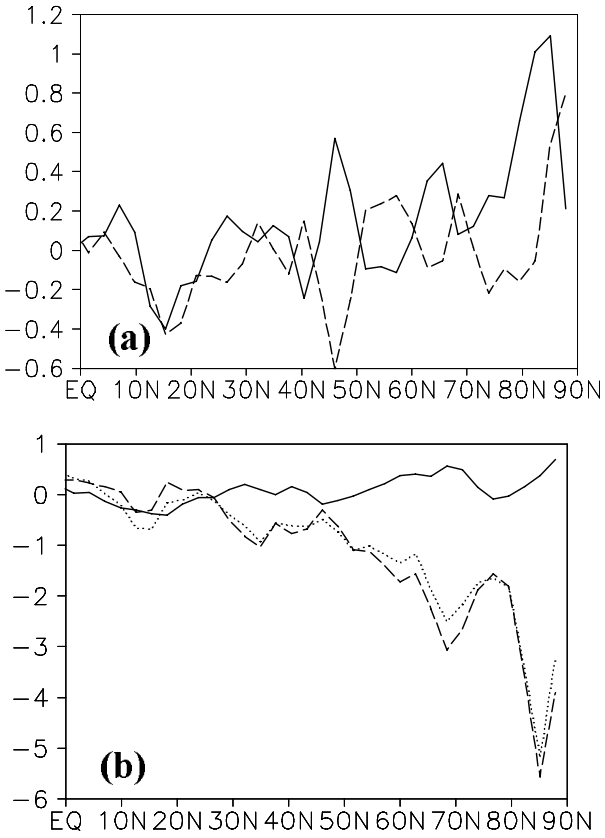

Fig. 4. The effect of BC in snow/ice on annual zonal means of (a) total cloud cover (%; dashed line) and net longwave flux at surface (units: W m^{-2}; solid line) and (b) shortwave cloud forcing (dashed line), longwave cloud forcing (solid line) and net cloud forcing (dot line; units: W m^{-2}).

and spring was ∼0.6°C. Two areas with large values were centered at 50°–70°N in February and at 70°–80°N in April, showing temperature increases of 1°C. The former could be caused by the model system errors, because it was not consistent with small surface radiative forcing during this time (Fig. 2b), and it had a low confidence level (t-test). At the Arctic pole, where perennial sea ice exists, the temperature of the sea-ice surface increased by >0.5°C in all seasons, with maximum increase of 2.5°C in September and October (Fig. 5a). Such increases will further accelerate ice melt in the Arctic. For regions north of the Arctic Circle, the surface temperature still increased during some periods without solar radiation, which may be a consequence of thermal inertia or could be dynamical in nature (Flanner et al., 2007). As shown in Fig. 5b, snowmelt rates obviously increased at the early melting stage in mid- and high-latitude areas of the North-

Table 1. Global and regional climate responses to BC in snow/ice.

	Surface radiative Forcing (W m^{-2})	Surface temperature (°C)	Snow cover ratio (10^{-3})	Snow depth (mm)	Ice amount on land (kg m^{-2})
Eurasia	0.57/0.90/0.42	0.83/0.60/0.39	–18.2/ – 26.2/ – 15.7	–12.6/ – 19.9/ – 13.6	–3.86/ – 8.02/ – 5.13
North America	0.26/0.44/0.19	0.83/0.46/0.47	–43.0/ – 33.5/ – 31.5	–27.2/ – 40.0/ – 26.2	–10.3/ – 20.8/ – 11.7
Global	0.013/0.094/0.025	0.094/0.089/0.071	–6.70/ – 8.65/ – 7.39	–8.91/ – 12.6/ – 10.7	–9.97/ – 14.5/ – 10.7

Note: *The three values represent the winter and spring seasons and the annual mean changes of these physical variables, respectively. The geographic ranges for Eurasia and North America are (30°–70°N, 20°–130°E) and (30°–70°N, 60°–130°W), respectively.

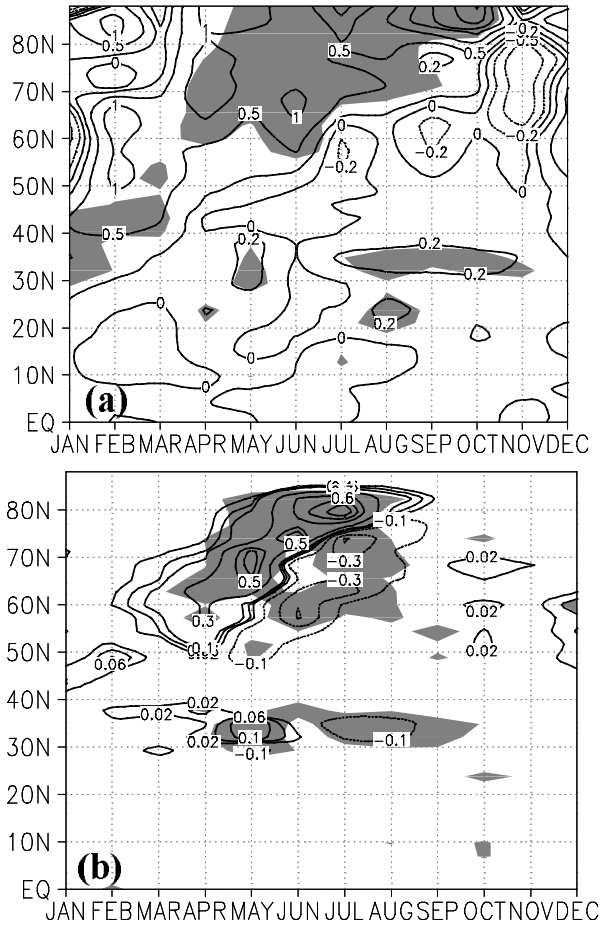

Fig. 5. Seasonal changes of zonal mean differences of (a) surface temperature (units: K) and (b) snow melt rate (units: mm d^{-1}) caused by the BC in snow/ice (The shaded areas shows the confidence exceeds 95% using a t-test).

ern Hemisphere, but they decreased due to the presence of less snow in the late melting stage. Corresponding to the temporal and spatial changes of temperature, the snowmelt rate on land in the Northern Hemisphere also increased obviously in winter and spring, which may shift peaks in river runoff to winter and early spring, away from summer and autumn when water demand is highest in these regions. Water storage capacities in these regions are not sufficient, and thus the earlier melting of snow/ice is expected to worsen water supply problems in the future (Barnett et al., 2005).

Eurasia and North America are the two major regions of snow cover on land, and increased snow/ice melting in these regions will have substantial impacts on local production and livelihoods. Table 1 lists the effects of BC in snow/ice on several important physical parameters worldwide and in the above two major snowpack regions. The seasonal mean values in winter and spring and the annual mean values of the snow cover ratio, snow depth, and ice amount in Eurasia and North America decreased due to the increased surface temperature. Flanner et al. (2009), from analysis of Jones (CRU) Air Temperature Anomalies Version 3 (CRUTEM3), showed that springtime surface temperatures on land north of 30°N over Eurasia and North America increased by 0.59°C (10 yr)$^{-1}$ and 0.23°C (10 yr)$^{-1}$, respectively, from 1979 to 2000. The surface temperatures increased by 0.6°C and 0.46°C over Eurasia and North America due to BC in snow/ice in this study, respectively, which could have contributed to the observational warming in those areas.

4. Conclusions

This study examined the radiative forcing of BC in snow/ice and its climatic effects by integrating the BC effects on snow/ice albedo calculated from observational data by Hansen and Nazarenko (2004) and Ming et al. (2009) into the BCC_AGCM2.0.1 developed by the NCC/CMA. Annual mean surface radiative forcing due to BC in snow/ice was calculated as approximately +0.042 W m^{-2}, which is smaller than the result reported by Hansen and Nazarenko (2004) because the impact of albedo is only considered at λ<0.7 μm in this work. The maximum annual mean surface forcing in

the Northern Hemisphere was shown over the Tibetan Plateau, where regional mean forcing exceeded +2.8 W m^{-2}; this finding is similar to that calculated by Flanner et al. (2007) using the BC emission list (Bond et al., 2004). At the two major regions of snow cover in Eurasia and North America, annual mean surface radiative forcing due to BC in snow/ice ranged from +0.2 W m^{-2} to approximately +2.0 W m^{-2}. In the Arctic, the mean value for sea ice was approximately +0.8 W m^{-2}. When simultaneously considering the BC in atmosphere, the ranges of positive surface forcing obviously decreased in Eurasia and North America, but it has hardly affected the forcing in Tibetan Plateau and Arctic pole.

Clear increases in surface temperatures were shown for land areas with snow cover and sea areas with ice cover due to the enhanced absorption of solar radiation caused by BC in snow/ice. The annual mean increases of temperature in snow-covered areas were estimated to be ∼1.6°C on the Tibetan Plateau, 0.5°C for most of Eurasia and North America, and >1°C in areas of northern Canada and the eastern United States. The corresponding zonal mean values around the Arctic pole reach 1°C, and the global annual mean value increased by 0.071°C. Therefore, with the rise of surface temperature in the Arctic, more water vapor could be released into the atmosphere, allowing for easier cloud formation, which could lead to higher thermal emittance arriving at the surface in the Arctic. However, the net cloud forcing could be decreased due to the increasing of cloud cover, which will offset some of the positive feedback mechanism of the clouds.

Positive surface radiative forcing by BC in snow/ice occurs in winter and spring, leading to increased surface temperature on land areas with snow and ice in the Northern Hemisphere. Surface temperatures of continental Eurasia and North America increased by 0.6°C and 0.46°C in spring, respectively. Corresponding to the seasonal changes of temperature, the snowmelt rate on land in the Northern Hemisphere clearly increased in winter and spring, which could lead to earlier peaks of river runoff in late winter and early spring. Because water storage capacities are not sufficient, much of the winter and spring runoff would flow directly to the oceans. Snow and ice water sources, which have already decreased, would be further lost to human use because the earlier peaks would not coincide with peak usage demands.

Finally, some uncertainty remains regarding sources in this study's simulations. First, the data of BC concentration in snow/ice were from limited sites; errors may be introduced by using the changes of albedos calculated in these sites to represent the changes of regional albedo. Second, the vertical distribution of BC in snow/ice, the mixed state of BC, and snow/ice particles and the climatic data set used to initialize and force the model may all affect the simulated results of this study. Therefore, we hope to obtain more data and more accurate parameterizations in the future and to apply them to further AGCM modeling.

Acknowledgements. This work was financially supported by the National Basic Research Program of China (Grant Nos. 2010CB955608 and 2011CB403405), the Public Meteorology Special Foundation of MOST (Grant No. GYHY200906020).

REFERENCES

Barnett, T. P., J. C. Adam, and D. P. Lettenmaier, 2005: Potential impacts of a warming climate on water availability in snow-dominated regions. *Nature*, **438**, 303–309.

Bond, T. C., D. G. Streets, K. F. Yarber, S. M. Nelson, J.-H. Woo, and Z. Klimont, 2004: A technology-based global inventory of black and organic carbon emissions from combustion. *J. Geophys. Res.*, **109**, D14203, doi: 10.1029/2003JD003697.

Briegleb, B. P., 1992: Delta-Eddington approximation for solar radiation in the NCAR Community Climate Model. *J. Geophys. Res.*, **97**, 7603–7612.

Collins, W. D., P. J. Rasch, B. E. Eaton, B. V. Khattatov, J.-F. Lamarque, and C. S. Zender, 2001: Simulating aerosols using a chemical transport model with assimilation of satellite aerosol retrievals: Methodology for INDOEX. *J. Geophys. Res.*, **106**, 7313–7336.

Collins, W. D., P. J. Rasch, B. E. Eaton, D. W. Fillmore, J. T. Kiehl, C. T. Beck, and C. S. Zender, 2002: Simulation of aerosol distributions and radiative forcing for INDOEX: Regional climate impacts. *J. Geophys. Res.*, **107**, doi: 10.1029/2001JD001365.

Flanner, M. G., C. S. Zender, P. G. Hess, N. M. Mahowald, T. H. Painter, V. Ramanathan, and P. J. Rasch, 2009: Springtime warming and reduced snow cover from carbonaceous particles. *Atmos. Chem. Phys.*, **9**, 2481–2497.

Flanner, M. G., C. S. Zender, J. T. Randerson, and P. J. Rasch, 2007: Present-day climate forcing and response from lack carbon in snow. *J. Geophys. Res.*, **112**, D11202, doi: 1 0.1029/2006JD008003.

Garrett, T. J., and C. Zhao, 2006: Increased Arctic cloud longwave emissivity associated with pollution from mid-latitudes. *Nature*, **440**, 787–789.

Grenfell, T. C., B. Light, and M. Sturm, 2002: Spatial distribution and radiative effects of soot in the snow and sea ice during the SHEBA experiment. *J. Geophys. Res.*, **107**(10), 8032, doi: 10.1029/2000JC000414.

Hansen, J., and L. Nazarenko, 2004: Soot climate forcing via snow and ice albedos. *Proc. Natl. Acad. Sci.*, **101**(2), 423–428.

Hansen, J., and Coauthors, 2007: Climate simulations for 1880–2003 with GISS modelE. *Climate Dyn.*, **29**,

661–696, doi: 10.1007/s00382-007-0255-8.

Harrison, E. F., P. Minnis, B. R. Barkstrom, V. Ramanathan, R. D. Cess, and G. G. Gibson, 1990: Seasonal variation of cloud radiative forcing derived from the earth radiation budget experiment. *J. Geophys. Res.*, **95**, 18687–18703.

IPCC, 2001: *Climate Change 2001: The Scientific Basis. Contribution of Working Group I to the Third Assessment Report of the Intergovernmental Panel on Climate Change*, Houghton et al., Eds., Cambridge University Press, Cambridge, 881pp.

IPCC, 2007: *Climate Change 2007: The Physical Science Basis. Contribution of Working Group I to the Fourth Assessment Report of the Intergovernmental Panel on Climate Change*, Solomon et al., Eds., Cambridge University Press, Cambridge, 131–217.

Jacobson, M. Z., 2004: Climate response of fossil fuel and biofuel soot, accounting for soot's feedback to snow and sea ice albedo and emissivity. *J. Geophys. Res.*, **109**, D21201, doi: 10.1029/2004JD004945.

Kistler, R., and Coauthors, 2001: The NCEP–NCAR 50–Year Reanalysis: Monthly means CD–ROM and documentation. *Bull. Amer. Meteor. Soc.*, **82**, 247–267.

Koch, D., S. Menon, A. D. Genio, R. Ruedy, I. Alienov, and G. A. Schmidt, 2009: Distinguishing aerosol impacts on climate over the past century. *J. Climate*, **22**, 2659–2677.

Light, B., H. Eicken, G. A. Maykut, and T. C. Grenfell, 1998: The effect of included particulates on the spectral albedo of sea ice. *J. Geophys. Res.*, **103**, 27739–27752.

Ming, J., H. Cachier, C. Xiao, D. Qin, S. Kang, S. Hou, and J. Xu, 2008: Black carbon record based on a shallow Himalayan ice core and its climatic implications. *Atmos. Chem. Phys.*, **8**, 1343–1352.

Ming, J., C. Xiao, H. Cachier, D. Qin, X. Qin, Z. Li, and J. Pu, 2009: Black Carbon (BC) in the snow of glaciers in west China and its potential effects on albedos. *Atmospheric Research*, **92**, 114–123.

Noone, K. J., and A. D. Clarke, 1988: Soot scavenging measurements in Arctic snowfall. *Atmos. Environ.*, **22**, 2773–2778.

Oleson, K. W., and Coauthors, 2004: Technical description of the community land model (CLM). Tech. Rep. NCAR/TN-461+STR, 174pp.

Rasch, P. J., N. W. Mahowald, and B. E. Eaton, 1997: Representations of transport, convection, and the hydrologic cycle in chemical transport models: Implications for the modeling of short lived and soluble species. *J. Geophys. Res.*, **102**, 28127–28138.

Rypdal, K., N. Rive, T. K. Berntsen, Z. Klimont, T. K. Mideksa, G. Myhre, and R. B. Skeie, 2009: Costs and global impacts of black carbon abatement strategies. *Tellus*, **61B**, 625–641.

Streets, D. G., and Coauthors, 2003: An inventory of gaseous and primary aerosol emissions in Asia in the year 2000. *J. Geophys. Res.*, **108**(D21), 8809, doi: 10.1029/2002JD003093.

Thompson, L. G., E. M. Thompson, M. E. Davis, P.-N. Lin, K. Henderson, and T. A. Mashiotta, 2003: Tropical glacier and ice core evidence of climate changes on annual to millenial time scales. *Climatic Change*, **59**, 137–155.

Wang, Z. L., H. Zhang, X. S. Shen, S. L. Gong, and X. Y. Zhang, 2010: A modeling study of aerosol indirect effects on global climate with an AGCM. *Adv. Atmos. Sci.*, **27**(5), 1064–1077, doi: 10.1007/s00376-010-9120-5.

Wang, Z. L., P. W. Guo, and H. Zhang, 2009: The numerical study of direct radiative forcing due to black carbon and its effects on the summer precipitation in China. *Climatic and Environmental Research*, **14**(2), 161–171. (in Chinese)

Warren, S., 1982: Optical properties of snow. *Rev. Geophys.*, **20**, 67–89.

Warren, S., and W. Wiscombe, 1980: A model for the spectral albedo of snow. II: Snow containing atmospheric aerosols. *J. Atmos. Sci.*, **37**, 2734–2745.

Wu, T., and G. Wu, 2004: An empirical formula to compute snow cover fraction in GCMs. *Adv. Atmos. Sci.*, **21**, 529–535.

Wu, T., and Coauthors, 2010: The Beijing Climate Center atmospheric general circulation model: Description and its performance for the present-day. *Climate Dyn.*, **34**, 123–147, doi: 10.1007/s00382-008-0487-2.

Xiao, C., and Coauthors, 2007: Observed changes of cryosphere in China over the second half of the 20^{th} century: An overview. *Annals of Glaciology*, **46**, 382–390.

Xu, B., T. Yao, X. Liu, and N. Wang, 2006: Elemental and organic carbon measurements with a two-step heating-gas chromatography system in snow samples from the Tibetan Plateau. *Annals of Glaciology*, **43**, 257–262.

Yan, H., 1987: Design of a nested fine-mesh model over the complex topograph, Part two: parameterization of the subgrid physical processes. *Plateau Meteorology*, **6**(Suppl.), 64–139. (in Chinese)

Zhang, G. J., and M. Mu, 2005: Effects of modifications to the Zhang-McFarlane convection parameterization on the simulation of the tropical precipitation in the National Center for Atmospheric Research Community Climate Model, version 3. *J. Geophys. Res.*, **110**, D09109, doi: 10.1029/2004JD005617.

Zhang, H., Z. L. Wang, P. W. Guo, and Z. Z. Wang, 2009: A modeling study of the effects of direct radiative forcing due to carbonaceous aerosol on the climate in East Asia. *Adv. Atmos. Sci.*, **26**(1), 57–66, doi: 10.1007/s00376-009-0057-5.